JMEPEG (2012) 21:2124–2130
DOI: 10.1007/s11665-012-0136-0

1059-9495/$19.00

Rate and Orientation Dependence of Formability in Fine-Grained AZ31B-O Mg Alloy Thin Sheet

Horng-Yu Wu, Pin-Hou Sun, Hung-Wei Chen, and Chui-Hung Chiu

(Submitted March 11, 2011; in revised form August 21, 2011)

Uniaxial tension and press forming tests were carried out at two different strain rates and temperatures to investigate the formability of fine-grained AZ31B-O Mg alloy thin sheet. Formability parameters were determined by tensile test results. The tensile properties and formability parameters were correlated with the forming limit diagrams. The present work focused on the effects of loading orientation and deformation rate on formability. Anisotropic behaviors were observed in the mechanical properties. Maximum strengths were obtained in the direction perpendicular to the rolling direction (RD). It can be concluded that the formability of the rolled fine-grained AZ31B-O Mg alloy sheet can be influenced by loading orientation and deformation rate. Stretch formability can be enhanced at a higher deformation rate, resulting from a lower anisotropy and a higher work hardening effect. In contrast, the drawing processes can be performed at a lower deformation rate to take advantage of a higher anisotropic behavior. Specimens with the RD parallel to the major strain in the press forming tests can enhance stretch formability, whereas specimens with the RD perpendicular to the major strain can improve deep-drawability.

Keywords anisotropy, fine-grained AZ31B-O Mg alloy, formability parameter, forming limit diagram

1. Introduction

Mg alloys are the lightest structural metallic alloys. They offer significant weight-reducing potential for various engineering applications because of their high specific strength and stiffness. The use of Mg alloys has been developed for electronic appliances and motor vehicle components (Ref 1, 2). Mg alloy products can be manufactured by casing, metal forming processes, and machining. Although die-casting is currently the major manufacturing process, low yield rates and gas porosity have led to the development of other processes. Press forming is considered as an alternative because of its relatively significant yield and performance. Among the Mg alloys, AZ31B-O alloy sheet is an interesting choice for use in the press forming process.

The formability of AZ31B-O alloy has been investigated (Ref 3-12). Agnew and Duygulu (Ref 3) examined the parameters that affect the practical sheet formability by conducting tensile tests on variously oriented specimens under different temperatures and strain rates. The examination showed that the strain hardening exponent is essentially constant up to 200 °C. At temperatures beyond this point, dynamic recrystallization processes cause a decrease in the hardening. Doege and Dröder (Ref 4) reported that the limit drawing ratio shows a considerable increase with lower punch speeds. Chino and Mabuchi (Ref 5) showed that stretch formability increases with the increase in grain size. Yukutake et al. (Ref 6) demonstrated that press formability of magnesium alloy sheets can be improved by decreasing the severity of the basal plane texture. Iwanaga et al. (Ref 7) and Chino et al. (Ref 8, 9) concluded that reduction of the (0 0 0 2) basal texture improves Erichsen values. The (0 0 0 2) basal planes in rolled Mg alloy sheets are intensively distributed parallel to the sheet plane. Under this condition, deformation of the textured sheets is difficult to achieve in the thickness direction under biaxial tension because the basal slip only occurs in the directions parallel to the sheet plane. Therefore, reduction of (0 0 0 2) texture can enhance straining in the thickness direction to improve Erichsen value. Chino et al. (Ref 10) showed that ductility, which is related to fine grain size, is an important factor for stretch formability at elevated temperature. The square cup drawing was demonstrated by Chen et al. (Ref 11). The results revealed that formability is improved as the die corner radius increases up to an optimum value. Lee et al. (Ref 12) showed that the work hardening exponent is an important property that prevents necking and improves sheet formability at elevated temperatures. Ravi Kumar et al. (Ref 13) indicated that a metal sheet with a higher value of normal anisotropy ($\bar{r}$) can promote good deep-drawability, and that a higher value of planar anisotropy (Δr) will increase the tendency of ear formation during drawing operations. Hosford (Ref 14) showed that $\bar{r}$ and its Δr values are highly dependent on texture. Despite all theses studies, however, the correlations between formability parameters and the forming limit diagrams (FLDs) have not been elucidated.

In this article, the formability of a commercially available fine-grained AZ31B-O alloy sheet is investigated using uniaxial tension and press forming tests under two temperatures and two

Horng-Yu Wu and **Hung-Wei Chen**, Department of Mechanical Engineering, Chung Hua University, 707, Sec. 2, Wufu Rd., Hsinchu 300, Taiwan; **Pin-Hou Sun**, Department of Mechanical Engineering, National Central University, 300, Jhongda Rd., Jhongli 320, Taiwan; and **Chui-Hung Chiu**, Material and Chemical Research Laboratories, Industrial Technology Research Institute, 195, Sec. 4, Chung Hsing Rd., Chutung 310, Taiwan. Contact e-mail: ncuwu@chu.edu.tw.

strain rates. The current work focused on the effects of loading orientation and strain rate on formability. In addition to the determination of basic mechanical properties, forming limit tests were performed to construct the FLD of the alloy. Formability was analyzed in relation to the mechanical properties and formability parameters.

2. Materials and Experimental Procedure

2.1 Materials

Magnesium Elektron North America Inc., USA, provided the Mg alloy AZ31B-O thin sheet with a thickness of 0.6 mm. The analyzed chemical composition (wt.%) was Mg-3.01Al-1.03Zn-0.21Mn. The microstructure of the as-received material was that of a relatively fine-grained structure. The average linear intercept grain size was approximately 7.5 μm before forming, as shown in Fig. 1.

2.2 Tensile Tests

The sheet-type tensile specimens, with a gauge length and width of 25 and 6 mm, respectively, were machined according to the ASTM B-557M standard procedure. Three types of tensile specimens were studied, namely, parallel to the rolling direction (RD), machined in the transverse direction (TD), and a specimen in an intermediate (45°) orientation. Uniaxial tension tests were carried out on three specimens for each direction at room temperature and 250 °C, using constant crosshead speeds which provide initial strain rates of 4×10^{-3} and 2×10^{-2} s^{-1}. The average values of the strengths, elongation, and work hardening exponent are evaluated based on

$$\text{Average} = \frac{X_{RD} + 2X_{45} + X_{TD}}{4} \quad \text{(Eq 1)}$$

where X represents either the yield strength (YS), ultimate tensile strength (UTS), elongation, or working hardening exponent.

The normal anisotropy or average plastic strain ratio ($\bar{r}$) and the planer anisotropy (Δr) were calculated from the r values (r is the plastic strain ratio which is the ratio of the width strain to the thickness strain) as determined along three directions, namely, parallel (RD), diagonal (45°), and perpendicular (TD) to the RD. The following expressions were used:

$$\bar{r} = \frac{r_{RD} + r_{TD} + 2r_{45}}{4} \quad \text{(Eq 2)}$$

$$\Delta r = \frac{r_{RD} + r_{TD} - 2r_{45}}{2} \quad \text{(Eq 3)}$$

2.3 Press Forming Tests

The press forming tests were performed for sheet specimens with different widths ranging from 10 to 100 mm (with increments of 10 mm) using a semi-spherical punch 50 mm in diameter, at room temperature and 250 °C. Increasing the width from 10 to 100 mm changes the state of stress from near balanced-biaxial tension through plane strain to uniaxial tension. The press forming tests were carried out at two punch speeds, namely, 6 and 30 mm/min. Punch speeds were kept constant during the tests. The punch was lubricated with graphite before testing. Two sets of specimens were prepared for press forming tests. In the first set, the length of the cut sheet was parallel to the RD; in the other set, the length of the sheet was perpendicular to the RD. Grid circles with a diameter d_o of 2.5 mm etched on the sheets were used to measure strain levels in each test. During forming, the etched circles were distorted into ellipses, and subsequently used to measure strain levels in each case. The major (d_1) and minor (d_2) diameters of the deformed circles after deformation were measured to determine the major strains (ε_1) and the minor strains (ε_2). Consequently, the major strains and the minor strains can then be expressed as:

$$\varepsilon_1 = \ln(d_1/d_o) \quad \text{(Eq 4)}$$

$$\varepsilon_2 = \ln(d_2/d_o). \quad \text{(Eq 5)}$$

The major and minor strains measured at the location closest to the fracture for each specimen were then plotted against each other with the major strain as the ordinate. The curve fitted on the strain points was defined as the forming limit curve. Considering a safety factor for design purposes, a 10% offset downward of the forming limit curve was adopted as the design curve.

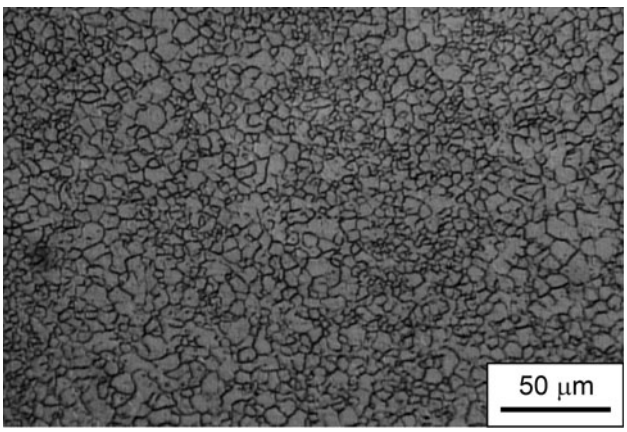

Fig. 1 Optical image of the microstructure of the fine-grained AZ31B-O Mg alloy

3. Results and Discussion

3.1 Tensile Properties

The stress-strain curves of the AZ31B-O alloy thin sheets are shown in Fig. 2 for RD and TD specimens for the testing at room temperature and 250 °C with two different strain rates. The values of the tensile properties at two different temperatures for each direction are given in Table 1 and 2. As the strain rate decreased, the ductility increased and the flow stress decreased. Plastic anisotropy in the mechanical properties was observed in the fine-grained Mg alloy AZ31B-O sheets. Maximum strengths were observed in the TD. The anisotropic behavior should be related to the crystallographic texture. The (0 0 0 2) pole figure of the as-received fine-grained AZ31B-O sheet, as obtained by X-ray diffraction, is given in Fig. 3. The figure indicates that most of the crystallites in the specimen were oriented with (0 0 0 2) plane in a nearly parallel manner in

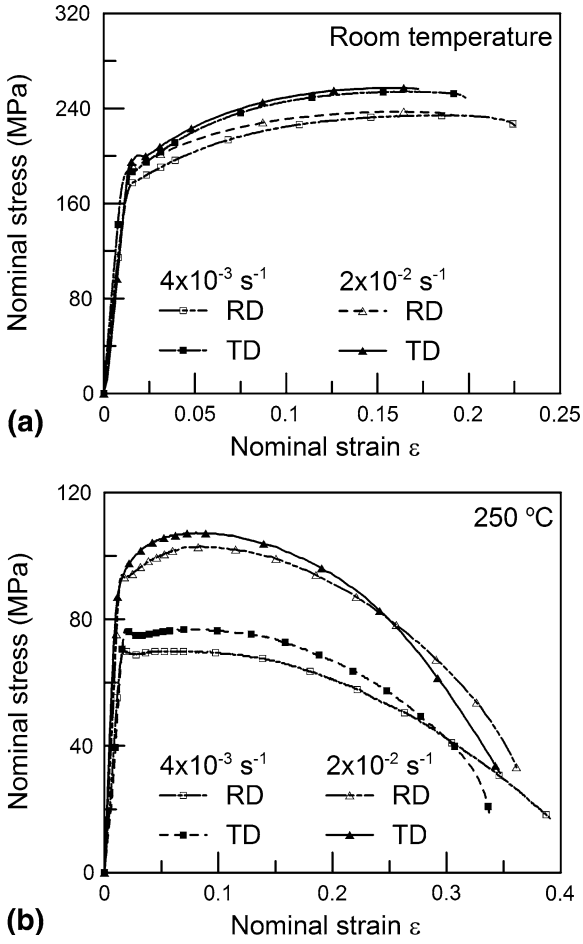

Fig. 2 Flow curves of the fine-grained AZ31B-O alloy sheets tested at two different initial strain rates for two different specimen orientations and temperatures: (a) room temperature, (b) 250 °C

relation to the rolling plane of the sheet. Accordingly, the *c*-axis of most grains was almost perpendicular to the plane of the sheet. Thus, the strong (0 0 0 2) basal texture caused anisotropy in mechanical properties. Similar results have been demonstrated by Koike (Ref 15).

Figure 2 also indicates that testing temperature influences the deformation behavior of the fine-grained AZ31B-O alloy sheet. The shape of the stress-strain curves changed significantly at 250 °C. The work hardening effect was low, and softening occurred at higher strains. The main strengthening process of AZ31B-O alloy is work hardening, whereas processes such as activation of non-basal slip, cross-slip, and climb of dislocations contribute to softening. Subsequently, the influence of temperature and strain rate on the deformation behavior can be related to the hardening and softening mechanisms. The dominant slip system in Mg and Mg alloys at room temperature is the $\langle a \rangle$ (basal) system. The activity of non-basal slip systems (pyramidal, prismatic) can occur at higher temperatures. The critical resolved shear stress (CRSS) of the non-basal slip systems of Mg and its alloys is dependent on temperature. The difference in CRSS between the basal plane slip and the non-basal plane slip decreases with increasing temperature (Ref 16). The activity of the non-basal slip systems plays an important role in softening. On one hand, the storage of dislocations at obstacles causes an increase in hardening. On the other hand, screw components of non-basal dislocations, $\langle c + a \rangle$, may move to the parallel slip planes through the double cross-slip followed by dislocation annihilation, causing a decrease in hardening (Ref 17). The fraction of $\langle c + a \rangle$ dislocations in Mg increases with increasing testing temperature, whereas the fraction of $\langle a \rangle$ dislocations decreases with increasing temperature. This was demonstrated by Máthis et al. (Ref 18) who also indicated that the activation of dislocation motion in the pyramidal system is energetically more favorable than twinning at temperatures above 200 °C.

Table 1 Tensile properties of the fine-grained AZ31B-O alloy sheet tested at room temperature

Strain rate	Orientation	YS, MPa	UTS, MPa	Elongation, %	*n*
4×10^{-3} s^{-1}	RD	171.3 ± 6.3	234.0 ± 7.2	22.6 ± 1.1	0.223 ± 0.014
	45°	183.3 ± 5.7	241.0 ± 6.9	20.9 ± 1.2	0.201 ± 0.013
	TD	185.0 ± 5.5	254.2 ± 6.1	19.9 ± 0.9	0.194 ± 0.016
	Average	180.7 ± 8.2	242.6 ± 9.6	21.1 ± 1.6	0.205 ± 0.020
2×10^{-2} s^{-1}	RD	191.7 ± 5.5	235.3 ± 7.8	19.3 ± 0.7	0.251 ± 0.018
	45°	193.6 ± 7.3	246.1 ± 8.8	18.6 ± 0.9	0.234 ± 0.015
	TD	195.4 ± 7.5	256.9 ± 8.1	17.6 ± 1.1	0.208 ± 0.020
	Average	193.6 ± 9.8	246.1 ± 11.8	18.5 ± 1.3	0.232 ± 0.022

Table 2 Tensile properties of the fine-grained AZ31B-O alloy sheet tested at 250 °C

Strain rate	Orientation	YS, MPa	UTS, MPa	Elongation, %	*n*
4×10^{-3} s^{-1}	RD	67.9 ± 3.7	69.8 ± 3.2	39.0 ± 1.9	0.074 ± 0.004
	45°	71.2 ± 3.1	72.6 ± 2.5	36.5 ± 2.1	0.065 ± 0.007
	TD	75.4 ± 2.9	76.8 ± 3.1	33.9 ± 1.7	0.061 ± 0.006
	Average	71.4 ± 4.5	73.0 ± 4.0	36.5 ± 2.8	0.066 ± 0.008
2×10^{-2} s^{-1}	RD	86.6 ± 5.1	102.7 ± 3.9	36.5 ± 0.7	0.150 ± 0.014
	45°	90.8 ± 3.5	105.6 ± 4.5	35.4 ± 0.9	0.130 ± 0.018
	TD	93.2 ± 3.7	107.1 ± 5.2	34.7 ± 0.9	0.115 ± 0.015
	Average	90.4 ± 5.6	105.3 ± 6.4	35.5 ± 1.2	0.131 ± 0.023

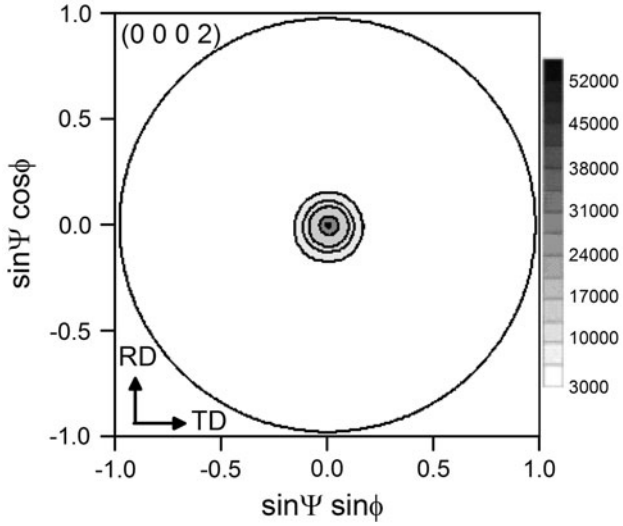

Fig. 3 Direct (0 0 0 2) pole figure performed by X-ray diffraction on the as-received specimen

One of the authors recently examined the tensile flow behavior of the fine-grained AZ31B-O Mg alloy thin sheet and determined a stress exponent of approximately 7 at 250 °C with strain rates from 4×10^{-3} to 1×10^{-1} s^{-1}. The result indicates that dislocation creep should be the deformation mechanism (Ref 19).

The minimum values of the work hardening exponent, n, (in the approximation of $\sigma = K\varepsilon^n$), were observed in the TD, and maximum values were found in the RD for all test conditions, as shown in Table 1 and 2. The average n value decreased with increasing temperature and decreasing strain rate. A metal sheet with a small n value will readily thin down locally before eventually fracturing during stretch forming. In contrast, when a metal sheet with a large n value is stretched, it will show the tendency toward strengthening due to work hardening effect, resulting in a more uniform change of sheet thickness. Local thinning of the sheet thickness is less likely to occur. A higher n value obviously supports stable plastic flow, thus promoting good stretch formability.

3.2 Formability Parameters

The formability parameters at two different strain rates of 4×10^{-3} and 2×10^{-2} s^{-1} determined by experiments are tabulated in Table 3 and 4. A metal sheet with a higher value of $\bar{r}$ (normal anisotropy) can promote good deep-drawability, and a higher Δr value (planar anisotropy) will increase the tendency of ear formation during drawing operation (Ref 13). Higher r values were observed in the TD in all test conditions. The fine-grained AZ31-O alloy sheet exhibited in-plane anisotropy even at 250 °C, whereas the r values and anisotropic behavior decreased at 250 °C. The r value in each direction for the testing at a higher strain rate of 2×10^{-2} s^{-1} was smaller than that at a lower strain rate of 4×10^{-3} s^{-1} under the same test temperature. The r values in the RD approached unity at 250 °C. Changes in the anisotropy with increasing temperature should be caused by an increase in activity of non-basal dislocations, $\langle c + a \rangle$, which enhance thinning effects in the thickness direction (Ref 3, 20).

Table 3 Formability parameters of the fine-grained AZ31B-O alloy sheet at room temperature

Strain rate	Orientation	r	nr
4×10^{-3} s^{-1}	RD	1.876	0.418
	45°	2.090	0.420
	TD	2.872	0.557
	Average	$\bar{r} = 2.232$	$\bar{n}\bar{r} = 0.455$
	Δr	0.284	
2×10^{-2} s^{-1}	RD	1.237	0.310
	45°	1.539	0.360
	TD	2.248	0.468
	Average	$\bar{r} = 1.641$	$\bar{n}\bar{r} = 0.381$
	Δr	0.204	

Table 4 Formability parameters of the fine-grained AZ31B-O alloy sheet at 250 °C

Strain rate	Orientation	r	nr
4×10^{-3} s^{-1}	RD	1.087	0.080
	45°	1.486	0.097
	TD	1.683	0.103
	Average	$\bar{r} = 1.418$	$\bar{n}\bar{r} = 0.094$
	Δr	−0.102	
2×10^{-2} s^{-1}	RD	1.066	0.160
	45°	1.281	0.167
	TD	1.475	0.170
	Average	$\bar{r} = 1.276$	$\bar{n}\bar{r} = 0.167$
	Δr	0.0105	

3.2.1 Formability Parameters at Room Temperature. The r values at room temperature and strain rate of 4×10^{-3} s^{-1} were 1.876 and 2.872 for the RD and TD specimens, respectively. The possibility of a rolled sheet with a low r value enhancing straining in the thickness direction is indicated. Therefore, the stretch formability of the RD specimen should be better than that of the TD specimen. This result is consistent with that of the study implemented by Chino et al. (Ref 8). A higher n value was also observed in the RD. If stretching predominates in the forming processes, n is the most important factor that influences stretch formability. A metal sheet with a high n value generally exhibits greater stretch formability (Ref 21). The RD specimen showed not only a lower r value but a higher n value as well, indicating that the stretch formability of the RD specimen should be better than that of the TD specimen at room temperature and under strain rate of 4×10^{-3} s^{-1}. Because the stress state of stretch forming is biaxial tension, the stress state of deep drawing approaches pure shear in the flange and the plane strain tension in the cup wall. A lower r value could improve stretch ability, but it would lead to lower deep-drawability. The planar anisotropy Δr was estimated to achieve a large positive value of 0.284 at room temperature and under strain rate of 4×10^{-3} s^{-1}. A large value of Δr indicates the high earing tendency of the alloy during deep drawing operation.

Similar results were also observed for the sheets tested at a higher initial strain rate of 2×10^{-2} s^{-1}. As the strain rate increased, the average n value increased and the $\bar{r}$ value decreased, indicating that stretch formability could be improved by increasing the forming rate. However, the decrease in

elongation and $\bar{r}$ value revealed that the increase in strain rate at room temperature was not favorable to deep-drawability.

The $\bar{r}$ values obtained at room temperature in the present work were 2.232 and 1.641 which were derived from the testing at 4×10^{-3} and 2×10^{-2} s^{-1}, respectively. Increasing strain rate would decrease $\bar{r}$ value, leading to the improvement of stretch formability. It is widely known that the formability of the Mg alloy sheet is dependent on the $\bar{r}$ value, which is related to the basal texture intensity (Ref 22-25). Chino et al. (Ref 10) investigated the stretch formability of AZ31 Mg alloy sheets at room temperature, and showed that specimens with lower texture intensity of (0 0 0 2), which results in lower $\bar{r}$ value, could improve stretch formability. Chino and Mabuchi (Ref 26) showed that the $\bar{r}$ value of the AZ31B alloy rolled at 723 K ($\bar{r} = 2.1$) is considerably lower than that of the specimen rolled at 663 K ($\bar{r} = 3.0$). Moreover, they demonstrated that stretch formability of AZ31B alloy at room temperature could be enhanced by rolling at 723 K. Huang et al. (Ref 27) demonstrated that the AZ31 alloy rolled at 823 K followed by rolling at 498 K exhibits a small $\bar{r}$ value of 0.89, which improved the capability of sheet thinning under the biaxial tension stress state of stretch forming. Huang et al. (Ref 28) indicated that increasing the rolling temperature from 723 to 828 K at the last rolling pass decreases the $\bar{r}$ values from 1.91 to 1.12, and that significant improvement in stretch formability could be achieved. Therefore, a rolled AZ31 sheet with weak (0 0 0 2) plane texture intensity exhibits low $\bar{r}$ value corresponding to enhancement of thickness-direction strain, which leads to improved stretch formability. In contrast, rolled AZ31 sheets with higher r value exhibit higher deep-drawability, as demonstrated by Agnew et al. (Ref 25).

Obtaining desirable $\bar{r}$ value for sheet metal forming is dependent on the forming process. The stress state of stretch forming is biaxial tension, where a lower $\bar{r}$ value will improve stretch formability. On the contrary, the stress state of deep drawing is close to pure shear in the flange and plane strain tension in the cup wall, where a higher $\bar{r}$ value would be more favorable to deep-drawability. Therefore, the results of the present work indicates that deforming a fine-grained AZ31B-O alloy sheet at a lower strain rate would enhance deep-drawability at room temperature, whereas stretch formability could be improved through deforming at a higher strain rate. In the present work, the values of planar anisotropy Δr estimated at room temperature were 0.284 and 0.204 derived from the testing at 4×10^{-3} and 2×10^{-2} s^{-1}, respectively. Δr value increased with increasing strain rate, and the values were relatively high for both test strain rates. These indicate that the tendency of ear formation was relatively high for the fine-grained AZ31-O alloy sheet at room temperature. Decreasing the strain rate might not be able to significantly improve the deep-drawability at room temperature.

3.2.2 Formability Parameters at 250 °C. The r values tested at 250 °C and under strain rate of 4×10^{-3} s^{-1} were significantly lower than those of the specimens tested at room temperature. Furthermore, the r value in the RD was close to unity. Although a drop in the average n value occurred at 250 °C, the stretch formability could still be improved based on the decrease in the $\bar{r}$ value and the increase in the average elongation. Compared with that in the TD, a low r value with a higher n value in the RD showed that the stretch formability in the RD remained superior to that in the RD at 250 °C. The r value in the RD was lower than that in the TD, which might result in a lower deep-drawability in the RD.

A small decrease in r value and a considerable increase in n value were observed in the RD at a higher strain rate of 2×10^{-2} s^{-1}, indicating that the stretch formability can be enhanced by using a higher strain rate. A lower r value with a higher n value in the RD showed that the stretch formability in the RD was higher than that in the TD at 250 °C and at a higher strain rate of 2×10^{-2} s^{-1}.

Table 4 shows that the $\bar{r}$ value also decreased with increasing strain rate for the testing at 250 °C. The $\bar{r}$ values obtained in the present work were 1.418 and 1.276 from the testing at 4×10^{-3} and 2×10^{-2} s^{-1}, respectively. These results are consistent with the $\bar{r}$ value of normal rolled AZ31 alloy specimens reported by Chino et al. (Ref 8) who showed that the $\bar{r}$ value from the testing at 220 °C and 1.7×10^{-3} s^{-1} is 1.58 for the normal rolled specimens. However, the $\bar{r}$ values in the present work are higher than those reported by Zhang et al. (Ref 29) and Chino et al. (Ref 9). A small $\bar{r}$ value of 0.90 in AZ31 alloy sheet from the testing at 240 °C and 1.4×10^{-2} s^{-1} was reported by Zhang et al. (Ref 29). The difference should be due to the variations in the initial microstructure or (0 0 0 2) plane texture intensity. The average grain size of the as-received specimen used in the present work was approximately 7.5 μm, whereas the average grain size of the hot-rolled sheet used in the work of Zhang was 4.5 μm. Chino et al. (Ref 9) showed that the reverse cross-rolled specimens has lower $\bar{r}$ value compared with that of the unidirectional cross-rolled specimens because the (0 0 0 2) plane texture intensity of the reverse cross-rolled specimen is lower than that of the unidirectional cross-rolled specimen. The values of $\bar{r}$ were approximately 1.12 and 1.33 for the reverse and unidirectional cross-rolled specimens from the testing at 220 °C and 1.7×10^{-3} s^{-1}, respectively. Therefore, higher $\bar{r}$ values observed in this work should be associated with the variations in the initial microstructure or (0 0 0 2) plane texture intensity.

Work hardening exponent n is also an important factor affecting stretch formability of a metal sheet. The n value can be considered as an index that would determine whether sheets are deformed uniformly or not; a lower n value indicates that uniform deformation in the thickness direction is not easy to achieve. Therefore, the $\bar{n}\bar{r}$ product can be used to evaluate the stretch formability of a metal sheet. Table 4 shows that the values of the $\bar{n}\bar{r}$ product were 0.09 and 0.17 from the testing at 4×10^{-3} and 2×10^{-2} s^{-1}, respectively. A reasonably high value of 0.17 for the $\bar{n}\bar{r}$ implied that the fine-grained AZ31B-O alloy sheet can likely tolerate moderate to fairly high limiting strains in the biaxial tension region on deforming at a higher strain rate of 2×10^{-2} s^{-1}.

3.3 Forming Limit Diagrams

3.3.1 Punch Speed of 6 mm/min. Fracture limit curves plotted as FLDs of the fine-grained AZ31B-O alloy sheet at two different temperatures and at a punch speed of 6 mm/min are displayed in Fig. 4. The RD-PMS designation in Fig. 4 means that the RD of the test piece is parallel to the major strain and the RD-TMS means that the RD is perpendicular to the major strain. Figure 4 indicates that both limiting strains were low under uniaxial and biaxial tension deformations at room temperature. In the biaxial tension region, the RD-PMS specimens showed higher major strains than RD-TMS specimens. As indicated in the tensile test results, the specimens tensioned in the RD exhibited high n and lower r values. Therefore, the stretch formability in the RD-PMS specimens

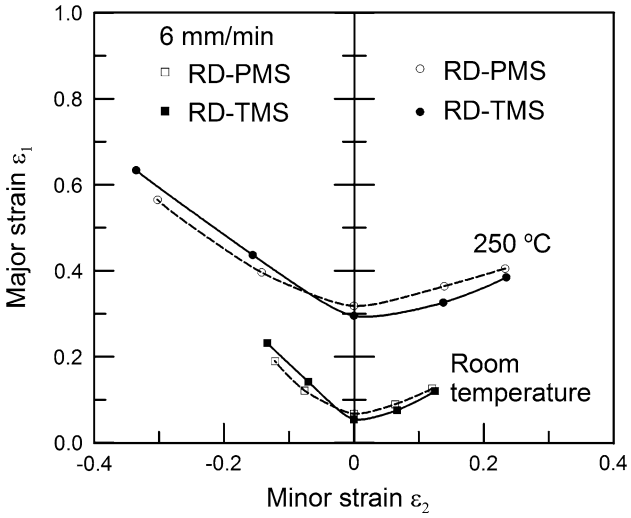

Fig. 4 Forming limit diagrams of the fine-grained AZ31B-O alloy sheets at a punch speed of 6 mm/min. RD-PMS: The rolling direction of the test piece is parallel to the major strain. RD-TMS: The rolling direction of the test piece is perpendicular to the major strain

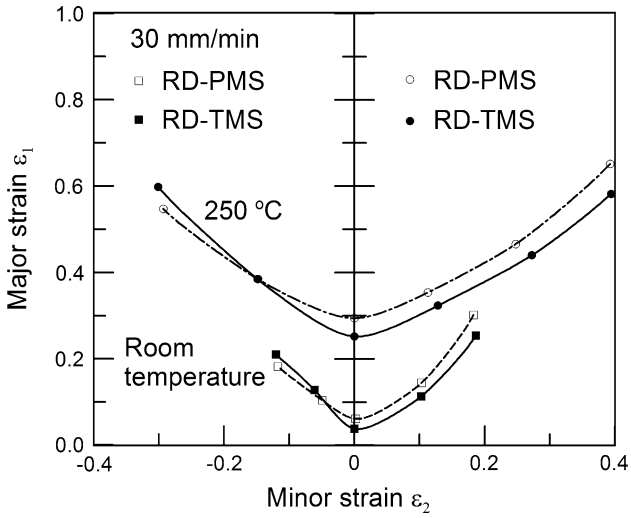

Fig. 5 Forming limit diagrams of the fine-grained AZ31B-O alloy sheets at a punch speed of 30 mm/min. RD-PMS: The rolling direction of the test piece is parallel to the major strain. RD-TMS: The rolling direction of the test piece is perpendicular to the major strain

was enhanced, leading to higher major strains in the biaxial tension region. Compared with RD-PMS specimens, RD-TMS specimens showed higher deep-drawability under uniaxial tensile stress, which is in agreement with the observation of TD specimens having higher r values in tensile tests. Although the fine-grained AZ31B-O sheet exhibits a respectable average ductility in the range of 18-21% at room temperature, its practical cold-stretch formability is limited because of basal texture (Ref 5).

Figure 4 also shows that the limiting strains under uniaxial tensile deformation increased significantly at 250 °C, whereas the limiting strains in the biaxial tension region increased much less. Although a decrease in $\bar{r}$ value was observed at 250 °C in the tensile test, a low average n value of 0.066 reduced the improvement in the stretch formability. The stretch formability was not significantly improved because of the noticeable decrease in n value at 250 °C. The thickness strain is necessary under a biaxial tension deformation, and obviously, a low n value does not support stable plastic flow. Thus, the stretch formability at 250 °C with a punch speed of 6 mm/min was not significantly enhanced. The RD specimens showed higher n and lower r values at 250 °C in tensile tests, resulting in higher stretch formability in the RD-PMS specimens. TD specimens with higher r values in the tensile tests showed higher deep-drawability in the RD-TMS specimens.

3.3.2 Punch Speed of 30 mm/min. The FLDs tested at a punch speed of 30 mm/min are illustrated in Fig. 5. In comparison with the specimens at a lower punch speed of 6 mm/min, increases in the limiting strains in the biaxial tension region were observed for the testing at room temperature. However, decreases in the limiting strains in the uniaxial tension region were found. These results are in agreement with forming parameters obtained from tensile tests, in which the $\bar{r}$ value decreased with increasing strain rate under the same deformation temperature. The FLDs shown in Figs. 4 and 5 indicate that a slight improvement of stretch formability could be reached using a higher punch speed at room temperature, whereas the deep-drawability would decrease.

At 250 °C with a punch speed of 30 mm/min, limiting strains in the biaxial tension region were significantly increased compared with the specimens deformed at a lower punch speed. The noticeable improvement of stretch formability was caused by the decrease in $\bar{r}$ value and the obvious increase in average n value, as revealed in the tensile tests. In contrast, decreases in limiting strains in the uniaxial tensile region were observed, which should be due to the decrease in the $\bar{r}$ value. Enhancement of straining in the thickness direction is necessary under the biaxial tension stress of stretch forming, and a smaller $\bar{r}$ value with a larger average n value could improve the sheet thinning capability. On the other hand, width strain can contribute to the total strain in the uniaxial tensile region with a larger $\bar{r}$ value. The RD-PMS specimens showed higher stretch formability at 250 °C because of their higher n and lower r values in the direction of the major strain, whereas the RD-TMS specimens with higher r values in the direction of the major strain exhibited higher deep-drawability.

Figure 5 illustrates good stretch formability observed in the biaxial tension region for the testing at 250 °C with a punch speed of 30 mm/min for both oriented specimens. Similar results were also reported by Chino et al. (Ref 10). Chino e al. (Ref 10) developed the FLDs in the biaxial tension region for five AZ31 Mg alloy specimens with different microstructures and texture intensities at 250 °C with a punch speed of 20 mm/min. The test specimens with smaller grain size tend to show higher forming limits, which is independent of texture intensity. Possibly, stretch formability at elevated temperatures could be enhanced using a sheet with high ductility accompanied by smaller grain size. Agnew et al. (Ref 3) showed that the in-plane strain anisotropy of an AZ31 Mg alloy for the testing at temperatures higher than 150 °C is significantly reduced, suggesting that dominate factor of stretch forming switches from plastic anisotropies to ductility with the increase in forming temperature. In comparison with the specimens deformed at 250 °C under a lower punch speed of 6 mm/min, the specimens deformed at a higher punch speed of 30 mm/min exhibit a lower $\bar{r}$ value, a higher average work

hardening exponent n, and similar ductility. These results lead to good stretch formability for both oriented specimens for the testing at 250 °C under a punch speed of 30 mm/min.

4. Conclusions

In the present study, analysis of the deformation behavior of a fine-grained AZ31B-O alloy using uniaxial tension and press forming tests was undertaken. The correlations between the formability parameters and the FLDs were analyzed. The increase in the deformation rate, which would increase the n value and decrease r value, could improve stretch formability. However, a decrease in the r value revealed that increase in deformation rate would not favor deep-drawability. The RD-PMS specimens with higher n values and lower r values in the major strain direction exhibited higher stretch formability, whereas the RD-TMS specimens with higher r values in the major strain direction revealed higher deep-drawability. Compared with specimens deformed at a lower punch speed of 6 mm/min, specimens subjected to a higher punch speed of 30 mm/min for the testing at 250 °C showed significantly enhanced stretch formability, which was a result of the decrease in the $\bar{r}$ value and the noticeable increase in the average n value.

Acknowledgments

This work was conducted through grants from National Science Council under the contract no. NSC 95-2212-E-216-009 and Chung Hua University under the contract no. CHU NSC 95-2212-E-216-009.

References

1. Y. Kojima and S. Kamado, Fundamental Magnesium Researches in Japan, *Mater. Sci. Forum*, 2005, **488–489**, p 9–16
2. R.S. Beals, C. Tissington, X.K. Zhang, J. Petrillo, M. Verbrugge, and M. Pekguleryuz, Magnesium Global Development: Outcomes from the TMS 2007 Annual Meeting, *J. Miner. Met. Mater. Soc.*, 2007, **59**, p 39–42
3. S.R. Agnew and Ö. Duygulu, Plastic Anisotropy and the Role of Non-basal Slip in Magnesium Alloy AZ31B, *Int. J. Plast.*, 2005, **21**, p 1161–1193
4. E. Doege and K. Dröder, Sheet Metal Forming of Magnesium Wrought Alloys—Formability and Process Technology, *J. Mater. Process. Technol.*, 2001, **115**, p 14–19
5. Y. Chino, K. Kimura, and M. Mabuchi, Deformation Characteristics at Room Temperature Under Biaxial Tensile Stress in Textured AZ31 Mg Alloy Sheets, *Acta Mater.*, 2009, **57**, p 1476–1485
6. E. Yukutake, J. Kaneko, and M. Sugamata, Anisotropy and Non-uniformity in Plastic Behavior of AZ31 Magnesium Alloy Plates, *Mater. Trans.*, 2003, **44**, p 452–457
7. K. Iwanaga, H. Tashiro, H. Okamoto, and K. Shimizu, Improvement of Formability from Room Temperature to Warm Temperature in AZ-31 Magnesium Alloy, *J. Mater. Process. Technol.*, 2004, **155–156**, p 1313–1316
8. Y. Chino, K. Sassa, A. Kamiya, and M. Mabuchi, Enhanced Formability at Elevated Temperature of a Cross-Rolled Magnesium Alloy Sheet, *Mater. Sci. Eng. A*, 2006, **441**, p 349–356
9. Y. Chino, K. Sassa, and A. Kamiya, Stretch Formability at Elevated Temperature of a Cross-Rolled AZ31 Mg Alloy Sheet with Different Rolling Routes, *Mater. Sci. Eng. A*, 2008, **473**, p 195–200
10. Y. Chino, H. Iwasaki, and M. Mabuchi, Stretch Formability of AZ31 Mg Alloy Sheets at Different Testing Temperatures, *Mater. Sci. Eng. A*, 2007, **466**, p 90–95
11. F.K. Chen, T.B. Huang, and C.K. Chang, Deep Drawing of Square Cups with Magnesium Alloy AZ31 Sheets, *Int. J. Mach. Tools Manuf.*, 2003, **43**, p 1553–1559
12. Y.S. Lee, M.C. Kim, S.W. Kim, Y.N. Kwon, S.W. Choi, and J.H. Lee, Experimental and Analytical Studies for Forming Limit of AZ31 Alloy on Warm Sheet Metal Forming, *J. Mater. Process. Technol.*, 2007, **187–188**, p 103–107
13. D. Ravi Kumar, A. Sen, and K. Swaminathan, The Formability and Texture Level of a Recent Automotive Stamping Grade Al-Mg-Mn Alloy, *J. Mater. Sci. Lett.*, 1994, **13**, p 971–973
14. W.F. Hosford, Reflections on the Dependence of Plastic Anisotropy on Texture, *Mater. Sci. Eng. A*, 1998, **257**, p 1–8
15. J. Koike, Enhanced Deformation Mechanisms by Anisotropic Plasticity in Polycrystalline Mg Alloys at Room Temperature, *Metall. Mater. Trans. A*, 2005, **36A**, p 1689–1696
16. H. Yoshinaga and R. Horiuchi, On the Nonbasal Slip in Magnesium Crystals, *Trans. JIM*, 1963, **5**, p 14–21
17. P. Lukác and Z. Trojanová, Hardening and Softening in Selected Magnesium Alloys, *Mater. Sci. Eng. A*, 2007, **462**, p 23–28
18. K. Máthis, K. Nyilas, A. Axt, I. Dragomir-Cernatescu, T. Ungár, and P. Lukáč, The Evolution of Non-basal Dislocations as a Function of Deformation Temperature in Pure Magnesium Determined by X-ray Diffraction, *Acta Mater.*, 2004, **52**, p 2889–2894
19. H.Y. Wu and W.C. Hsu, Tensile Flow Behavior of Fine-Grained AZ31B Magnesium Alloy Thin Sheet at Elevated Temperatures, *J. Alloys Compd.*, 2010, **493**, p 590–594
20. A. Jäger, P. Lukáč, V. Gärtnerová, J. Bohlen, and K.U. Kainer, Tensile Properties of Hot Rolled AZ31 Mg Alloy Sheets at Elevated Temperatures, *J. Alloys Compd.*, 2004, **378**, p 184–187
21. R. Narayanasamy and C. Sathiya Narayanan, Forming Limit Diagram for Interstitial Free Steels. Part I, *Mater. Sci. Eng. A*, 2005, **399**, p 292–307
22. X.S. Huang, K. Suzuki, A. Watazu, I. Shigematsu, and N. Saito, Improvement of Formability of Mg-Al-Zn Alloy Sheet at Low Temperatures Using Differential Speed Rolling, *J. Alloys Compd.*, 2009, **470**, p 263–268
23. S. Yi, J. Bohlen, F. Heinemann, and D. Letzig, Mechanical Anisotropy and Deep Drawing Behaviour of AZ31 and ZE10 Magnesium Alloy Sheets, *Acta Mater.*, 2010, **58**, p 592–605
24. T. Al-Samman, Comparative Study of the Deformation Behavior of Hexagonal Magnesium-Lithium Alloys and a Conventional Magnesium AZ31 Alloy, *Acta Mater.*, 2009, **57**, p 2229–2242
25. S.R. Agnew, J.W. Senn, and J.A. Horton, Mg Sheet Metal Forming: Lessons Learned from deep drawing Li and Y Solid-Solution Alloys, *J. Miner. Met. Mater. Soc.*, 2006, **58**, p 62–69
26. Y. Chino and M. Mabuchi, Enhanced Stretch Formability of Mg-Al-Zn Alloy Sheets Rolled at High Temperature (723 K), *Scripta Mater.*, 2009, **60**, p 447–450
27. X. Huang, K. Suzuki, and N. Saito, Enhancement of Stretch Formability of Mg-3Al-1Zn Alloy Sheet Using Hot Rolling at High Temperatures up to 823 K and Subsequent Warm Rolling, *Scripta Mater.*, 2009, **61**, p 445–448
28. X. Huang, K. Suzuki, Y. Chino, and M. Mabuchi, Improvement of Stretch Formability of Mg-3Al-1Zn Alloy Sheet by High Temperature Rolling at Finishing Pass, *J. Alloys Compd.*, 2011, **509**, p 7579–7584
29. K.F. Zhang, D.L. Yin, and D.Z. Wu, Formability of AZ31 Magnesium Alloy Sheets at Warm Working Conditions, *Int. J. Mach. Tools Manuf.*, 2006, **46**, p 1276–1280